Topological and spatial aspects of the hydration of solutes of extreme solvation entropy

Dan L. Bergman,* Alexander P. Lyubartsev, and Aatto Laaksonen
Division of Physical Chemistry, Arrhenius Laboratory, Stockholm University, SE-106 91 Stockholm, Sweden
(Received 16 April 1999; revised manuscript received 14 June 1999)

The hydration of charged Lennard-Jones spheres by simple point charge water is considered. Molecular dynamics and expanded ensemble simulations were used to compare the hydration structures surrounding solutes with extreme solvation entropy. The variations in the solvation entropy were analyzed in terms of changes in the spatial and topological structure of the hydration shells. The solvation entropy was found to be maximal for solutes that can replace water molecules in the hydrogen-bond network. Further, using a Kirkwood-type factorization, the solvation entropy was expanded as a sum over the partial *n*-body distribution functions. The two-body solute-water contribution to the solvation entropy was found to exceed the full solvation entropy for solutes with low charge, whereas the converse is true for the other solutes. This is consistent with the idea that water-water correlations are enhanced by solvation of, for example, noble gases, whereas they are disrupted by solvation of ions. Further, the orientational and radial parts of the two-body solute-water entropy were calculated as functions of the charge of the solute. The orientational part has a single maximum, whereas the radial part maintains the bimodal form of the full solvation entropy.
[S1063-651X(99)13110-6]

PACS number(s): 61.20.Qg, 65.50.+m, 61.20.Ja

I. INTRODUCTION

Simple solutes such as noble gases and atomic ions are hydrated differently depending on (among other things) their size and charge [1–3]. A large number of simulations have been carried out in order to study various aspects of the hydration of solutes of this type [4–13]. In these simulations, a plentitude of different potential models of varying complexity have been used to represent the water-water, water-solute, and solute-solute interactions [7–9,14,15]. Recently, Lynden-Bell and Rasaiah [4] carried out expanded ensemble simulations where the size and charge of the solutes were varied continuously. This enabled them to move smoothly between different types of hydration, and to identify solutes corresponding to extrema in the solvation entropy; see Fig. 1.

With the present paper we extend their analysis of the hydration structures surrounding these extreme solutes in two directions: first, we look at the angular structure of the hydration shells and, second, we look at changes in the topology of the hydrogen-bond network. A clear picture of the relation between changes in the solvation entropy, on the one hand, and changes in the solvation structure, on the other hand, is obtained by comparing the hydration of these extreme solutes. Further, using a Kirkwood-type [16] factorization of the *N*-particle distribution function, we have expanded the solvation entropy in a sum over the partial *n*-particle distribution functions [17,18]. This allows us to interpret the solvation entropy in terms of contributions from different types of spatial correlations.

The paper is arranged as follows: In Sec. II we describe our simulation model, and consider to what extent it mimics solvation at infinite dilution. In Secs. III and IV, the spatial and topological structures of the hydration shells are analyzed. Contributions from different types of spatial correlations to the solvation entropy are considered in Sec. V, and the dynamics of the exchange of water molecules betweenthe solvation shells and the bulk is briefly considered in Sec. VI. Section VII concludes the paper.

II. SIMULATIONS AND MODEL

The incentive for our work was the solvation entropies calculated by Lynden-Bell and Rasaiah [4]. Our simulations were therefore set up to resemble theirs as closely as possible with the following two exceptions: Lynden-Bell and Rasaiah simulated the solute together with 63 water molecules using

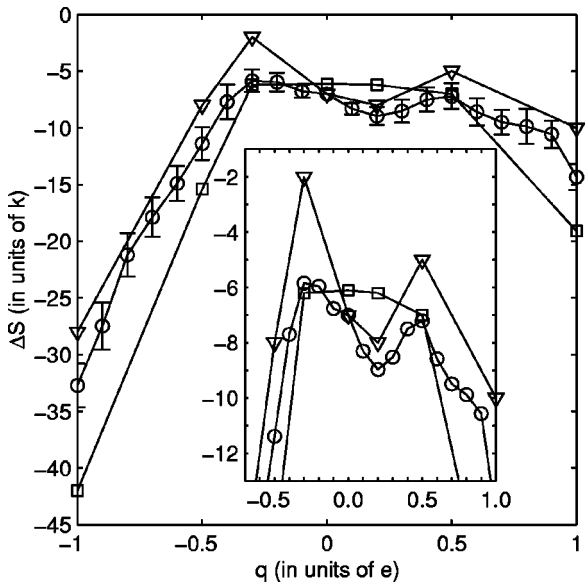

FIG. 1. The solvation entropy ΔS in units of Boltzmann's constant k for solutes of different charge q: ○ denotes our expanded ensemble data, ▽ Lynden-Bell and Rasaiah's data [4], and □ the two-body solute-water contribution $S_{sw}^{(2)}$ to ΔS [cf. Eq. (12a) and Table VI]. The error bars indicate one standard deviation. The errors in $S_{sw}^{(2)}$ are discussed in Sec. V.

*Author to whom correspondance should be addressed. Electronic address: dan@physc.su.se

TABLE I. Different energies. q denotes the charge of the solute, E_{tot} the total potential energy of the system, E_{sw} the contribution from the solute-water interactions, and E_{ww} the contribution from the water-water interactions. ΔF is the solvation free energy relative to the $q=0$ solute (i.e., $\Delta F = F_q - F_0$). All energies are in kJ/mol. E_{tot} and E_{ww} are per molecule (there are 256 molecules in each system). The estimated standard deviation is either less than one unit in the last digit or given within the parentheses. E_{sw} and E_{ww} only contain contributions from pairs separated by less than $L/2$, where L is the side length of the simulation cell. [The energy per molecule in the pure water simulation is -46.65 kJ/mol (there are 255 molecules in the system)].

	$q(e)$						
	-1.0	-0.5	-0.3	0.0	$+0.2$	$+0.5$	$+1.0$
ΔF	$-592.8(5)$	$-142.0(3)$	$-48.3(2)$	0	$-2.65(7)$	$-46.8(2)$	$-251.5(3)$
E_{tot}	-49.41	-47.16	-46.68	-46.49	-46.52	-46.76	-47.90
E_{ww}	-47.15	-48.62	-48.92	-49.29	-49.27	-48.84	-47.87
E_{sw}	$-1180(4)$	$-302(2)$	$-101(1)$	$-3.83(2)$	$-20.0(5)$	$-138(2)$	$-617(3)$

face centered cubic (fcc) boundary conditions (that is, the simulation cell subjected to periodic boundary conditions was a rhombic dodecahedron). We have simulated the solute together with 255 water molecules using simple cubic (sc) boundary conditions.

We have carried out seven molecular dynamics simulations of simple charged Lennard-Jones solutes surrounded by rigid simple point charge (SPC/E) water molecules [19]. The simulations differed only in that the charge q of the solute was varied. Solutes of charge $q=-1,-0.5,-0.3,0,+0.2,+0.5$, and $+1$ (in units of the electron charge e) were selected, since they correspond to extrema and other interesting points on the solvation entropy curve; see Fig. 1. We have also simulated a pure water system consisting of 255 molecules.

The electrostatic part of the interaction potential was evaluated using Ewald summation; see below. The Lennard-Jones part of the potential was determined by the parameters $\sigma=2.586$ Å and $\epsilon=0.4184$ kJ/mol for the solute, and $\sigma=3.166$ Å and $\epsilon=0.6502$ kJ/mol for the SPC/E water. The mixed potential terms were calculated using the Lorentz-Berthelot combination rules. The mass of the solute was 22.9898 g/mol. As Lynden-Bell and Rasaiah pointed out, these are reasonable potential parameters for simulation of sodium ions in water.

The simulations were carried out in the canonical ensemble at $T=298.15$ K and $\rho=1.00868$ g/cm^3. The ρ selected corresponds to a simulation cell with a side length $L=19.6611$ Å. A Nose-Hoover thermostat [20] with a relaxation time of 30 fs was used to maintain the temperature and the time step was two femtoseconds. The Shake algorithm [21] was used to keep the bond lengths fixed. Each simulation consisted of a 200-ps-long equilibration run followed by a 2-ns-long production run. The simulations were performed using the simulation package MDYNAMIX [22]. The simulation of the pure water system was set up in the same way as the other (note that L was kept at 19.6611 Å, whereas the density was adjusted accordingly).

Lynden-Bell and Rasaiah's [4] expanded ensemble simulations show that the solvation entropy varies bimodally with the solute's charge. We have carried out an expanded ensemble simulation to see if the solvation entropy varies bimodally with the charge also for our larger system. Figure 1 shows that this is the case. Further, the locations of the extrema are the same, but the differences between the maxima and the minimum are smaller. The estimated standard deviation of the change in the solvation entropy ranges from $0.5k$ to $2k$, depending on the charge of the solute (see Fig. 1). Note that we have only calculated the difference in the solvation entropy between the $q=0$ and the other solutes. We have also calculated the solvation free energy; see Table I.

Our expanded ensemble consisted of 21 canonical systems differing only in that the charge of the solute was varied between -1 and $+1$ in steps of 0.1. The expanded system was simulated using a combined Monte Carlo (MC) and molecular dynamics (MD) approach [25,26]. Briefly, the transitions between the subensembles were done using a Metropolis MC algorithm, and within the subensembles ordinary MD steps were taken. A biasing potential was used to ensure that efficient acceptance ratios were obtained for the transitions between the subensembles. In total 4.5×10^5 transitions were made between the subensembles, and 7×10^6 MD steps were taken within the subensembles. The MD steps were 2 fs long. The density, temperature, and other simulation parameters were the same as for the MD simulations described above.

In order to compare the hydration structures that we obtain for our sc system with those that Lynden-Bell and Rasaiah obtained for their smaller fcc system; we have calculated $g_{SO}(r)$, that is the radial distribution functions of oxygen atoms surrounding the solute (see Fig. 2), and the average charge density surrounding the solute. On comparing these distributions with those obtained by Lynden-Bell and Rasaiah, we find no significant differences.

As all solutes that we simulate (except one) are charged, a uniform continuum charge density of opposite sign has been introduced in order to maintain a net charge of zero in the simulation cell. This continuum need not be explicitly accounted for when calculating the forces, since it only contributes an extra constant term to the electrostatic part of the potential energy,

$$U_{el}=\sum_{i<j} q_i q_j \psi(\mathbf{r}_i-\mathbf{r}_j) - \sum_{i<j,\text{intra}} \frac{q_i q_j}{|\mathbf{r}_i-\mathbf{r}_j|} + \frac{\xi}{2}\sum_i q_i^2 - \frac{\pi}{2V\kappa^2} q_b^2, \qquad (1)$$

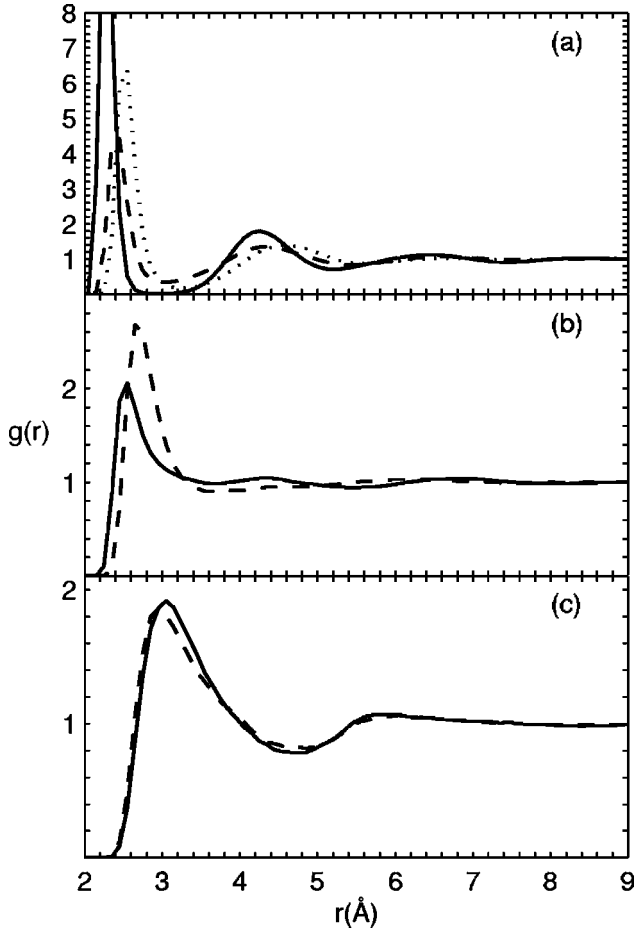

FIG. 2. Radial distribution functions $g(r)$ of oxygen atoms surrounding the solute. (a) Distributions for solutes of charge $q=-1$ (solid line), $q=+1$ (dashed line), and $q=-0.5$ (dotted line). (b) Distributions for solutes of charge $q=-0.3$ (solid line) and $q=+0.5$ (dashed line). (c) Distributions for solutes of charge $q=0$ (solid line) and $q=+0.2$ (dashed line). The maximum value of $g(r)$ for the $q=-1$ solute is 12.4. Compare Fig. 5 in Ref. [4].

where

$$\psi(\mathbf{r})=\sum_{\mathbf{R}}\frac{\operatorname{erfc}(\kappa|\mathbf{r}+\mathbf{R}|)}{|\mathbf{r}+\mathbf{R}|}+\frac{1}{V}\sum_{\mathbf{G}\neq 0}\frac{1}{\pi G^2}\exp\left(2\pi i\mathbf{G}\mathbf{r}-\frac{\pi^2G^2}{\kappa^2}\right) \tag{2}$$

and

$$\xi=\sum_{\mathbf{R}\neq 0}\frac{\operatorname{erfc}(\kappa R)}{R}+\frac{1}{V}\sum_{\mathbf{G}\neq 0}\frac{1}{\pi G^2}\exp\left(-\frac{\pi^2G^2}{\kappa^2}\right)-\frac{2\kappa}{\sqrt{\pi}}. \tag{3}$$

Above, q_i denotes the size, and $\mathbf{r}_i$ the position of the ith charge. The first summation in Eq. (1) is carried out over all charge pairs, whereas the second is only carried out over those located in the same molecule. $\mathbf{R}$ denotes the real space lattice vectors and $\mathbf{G}$ the reciprocal. Since we consider a simple cubic lattice, $\mathbf{R}$ takes the values $L\mathbf{n}$, where $\mathbf{n}$ is an arbitrary integer triplet and L is the side length of the simulation cell. The $\mathbf{G}$'s have been normalized to satisfy the relation $\mathbf{R}\cdot\mathbf{G}=n$ for some integer n. V denotes the volume of the unit cell, κ is an arbitrary positive constant [regulating the rate of convergence of the two parts of (2)], and q_b is the total charge of the continuum. Note that the three first terms in Eq. (1) are equal to the expression derived by de Leeuw *et al.* [23] for a spherical cluster of cells minus the dipole term. Physically, the neglect of the dipole term amounts to placing the spherical cluster inside a perfect conductor (tinfoil boundary conditions). As the dipole term is the only nonperiodic part of the potential, it is clear that the shape of the cluster no longer is relevant when tinfoil boundary conditions are applied. The fourth term is the contribution from the continuum; see for example Appendix A in Ref. [24].

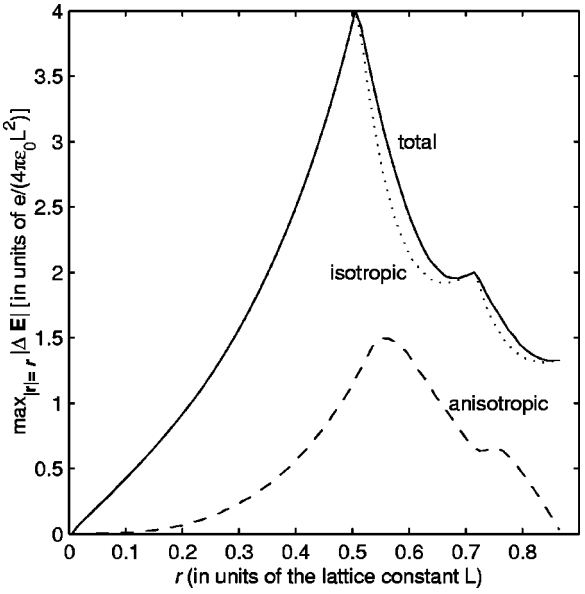

FIG. 3. The absolute difference between the electric field surrounding a point charge in a simple cubic Wigner crystal $\mathbf{E}_{\mathrm{sc}}$ and the electric field surrounding an isolated point charge $\mathbf{E}_{\mathrm{co}}$. For each distance r from the solute, the maximal difference between the electric fields, the maximal isotropic difference, and the maximal anisotropic difference are plotted. Formally, these differences are given by $\max_{|\mathbf{r}|=r}|\Delta\mathbf{E}|$, where $\Delta\mathbf{E}=\Delta\mathbf{E}_{\mathrm{tot}}$, $\Delta\mathbf{E}_{\mathrm{iso}}$, and $\Delta\mathbf{E}_{\mathrm{aniso}}$, respectively; and where $\Delta\mathbf{E}_{\mathrm{tot}}=\mathbf{E}_{\mathrm{sc}}-\mathbf{E}_{\mathrm{co}}$, $\Delta\mathbf{E}_{\mathrm{iso}}=\mathbf{e}_r(\mathbf{e}_r\cdot\Delta\mathbf{E}_{\mathrm{tot}})$, and $\Delta\mathbf{E}_{\mathrm{aniso}}=\Delta\mathbf{E}_{\mathrm{tot}}-\Delta\mathbf{E}_{\mathrm{iso}}$. $\mathbf{e}_r$ denotes the radial unit vector.

In order to calculate the solvation energy of the solute, it is necessary to account for the cohesive energy associated with the formation of a simple cubic Wigner lattice [4,6] consisting of the solute and a uniform neutralizing continuum. The cohesive energy associated with the Wigner lattice can be obtained by evaluating Eq. (1) for a single point charge. U_{el} then sums to $-q_b^2/(2L)\times 2.837\,297\,479\,48$.

One objective of our simulations is to learn something about the solvation of ions at infinite dilution. It is therefore interesting to consider the differences between the electric field surrounding a point charge in a simple cubic Wigner crystal $\mathbf{E}_{\mathrm{sc}}$, and the electric field surrounding an isolated point charge $\mathbf{E}_{\mathrm{co}}$. As the maximal relative difference in the electric field at a given distance r from the solute, that is

$$\max_{|\mathbf{r}|=r}|\mathbf{E}_{\mathrm{sc}}-\mathbf{E}_{\mathrm{co}}|/|\mathbf{E}_{\mathrm{co}}|, \tag{4}$$

is less than 0.1 for distances up to than 5.3 Å (that is $0.27L$),

we expect the electric field sensed by the water molecules in this region to be sufficiently similar to that generated by a single point charge at infinite dilution. By sufficiently similar we mean that the structure and dynamics of the water molecules in this region are not significantly influenced by the differences between $\mathbf{E}_{sc}$ and $\mathbf{E}_{co}$. At larger distances ($r > 0.27L$), the relative difference increases. However, the typical electric field sensed by a water molecule from its nearest neighbors is about 60 $e/(4\pi\epsilon_0 L^2)$, to be compared with $|\Delta\mathbf{E}|$, which is less than 4 $e/(4\pi\epsilon_0 L^2)$ everywhere in the simulation cell for a solute of charge $q=1$; see Fig. 3. Further, the water molecules in the first solvation shell screen the solute's charge to some extent. Thus we do not expect $\Delta\mathbf{E}$ to induce any significant structural or dynamical changes for $r > 0.27L$.

III. SPATIAL ARRANGEMENT

We have calculated the solute-oxygen and solute-hydrogen radial distribution functions (see Fig. 2 for the solute-oxygen distributions). From these distributions we have also calculated the charge distribution surrounding the solute. As has already been mentioned in Sec. II, these distributions do not differ significantly from those previously obtained by Lynden-Bell and Rasaiah [4].

In order to obtain a clearer picture of the hydration structure, we have looked at the orientation of water molecules at different distances r from the solute. For each distance r, the angular distribution function $a(r,\theta,\phi)$ has been calculated (θ and ϕ are defined in Fig. 4). These distributions have been normalized to 4π, that is the surface of the unit sphere. Thus, if all orientations were equally probable, the distribution function would be uniformly equal to 1. The distribution functions describing the orientation of the water molecules in the first solvation shell are shown in Fig. 5.

Considering the negatively charged solutes first, we expect the water molecules in the first hydration shell to bond via one of their protons to the solute. The maxima at $\cos\theta = 0.6$ and $\phi = \pi/2$ confirm this. As the solute's charge increases from -1 to -0.3, the water molecules gain orientational freedom: the angular distribution broadens significantly, and its maximum value decreases from 111 to 21. For

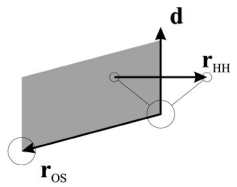

FIG. 4. Definition of $\cos\theta$ and ϕ. $\cos\theta$ is the cosine of the angle between the dipole moment of the water molecule **d** and the vector from the water molecule's oxygen atom to the solute, $\mathbf{r}_{OS}$. ϕ is the angle between the plane spanned by the water molecule and the plane spanned by the **d** and $\mathbf{r}_{OS}$ vectors minus $\pi/2$. Let **e** denote a unit vector; then we formally have $\cos\theta = \mathbf{e}_d \cdot \mathbf{e}_{OS}$ and $\sin\phi = (\mathbf{e}_d \times \mathbf{e}_{OS}) \cdot (\mathbf{e}_d \times \mathbf{e}_{HH})$.

solutes with charges 0 and $+0.2$, the angular distributions are considerably flatter, the global maxima are 2.5 and 2.7, respectively. As the charge increases further to $+0.5$ and $+1$, the water dipoles are forced to align themselves with the central electric field. For the $+0.5$ solute, the maximum is 4.2, and it is located at $\cos\theta = -0.6$ and $\phi = 0$; for the $+1$ solute, the maximum is 9.9, and it is located at $\cos\theta = -1$ and $\phi = 0$. It is clear that the closer the water molecule aligns its dipole to the central electric field, the more freedom it gains for rotation around its dipole axis.

If we know the most probable orientation of a water molecule in the first solvation shell, then we also know the most probable position of the solute relative to the water molecule. Taking this point of view, one may notice that the $q = -0.3$ and $+0.5$ solutes both coordinate tetrahedrally relative to the water molecule. Thus the solutes associated with maxima in the solvation entropy are precisely those that can ''fit'' into the hydrogen-bond network. (The $q = -0.5$ and -1 solutes have the correct orientation, but their distance to the water molecule is less than 2.6 Å; see the distances in Table IV). From this point of view it is also easier to interpret the $q = 0$ and $+0.2$ distributions: There is a high probability of finding these solutes in the leftover, that is, the nontetrahedral, positions. Integration of g_{SO} shows that there are about four closest coordinated water molecules surrounding the $q = -0.3$ and $+0.5$ solutes. Integration of $a(r,\theta,\phi)$ shows that about two of these four water molecules coordinate the solute tetrahedrally. The remaining two water mol-

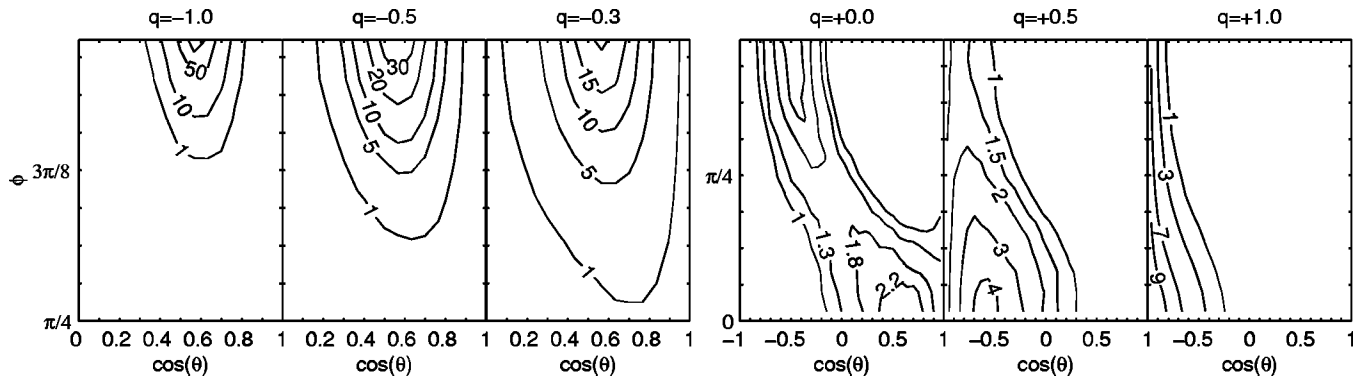

FIG. 5. Angular distribution functions $a(r,\theta,\phi)$ describing the orientation of the water molecules in the first solvation shell (i.e., the 0.2-Å-thick spherical shell centered at the maximum, $r = r_{max}$, of the solute-oxygen radial distribution function). The distributions have been normalized to 4π. Thus, if all orientations were equally probable, the distribution function would be uniformly equal to 1. $\cos\theta$ and ϕ are defined in Fig. 4. Because of the water molecule's symmetry only $0 \leq \phi \leq \pi/2$ need to be considered. For the negatively charged solutes, $a(r,\theta,\phi)$ is less than 1 when $\phi \leq \pi/4$ or $\cos\theta \leq 0$.

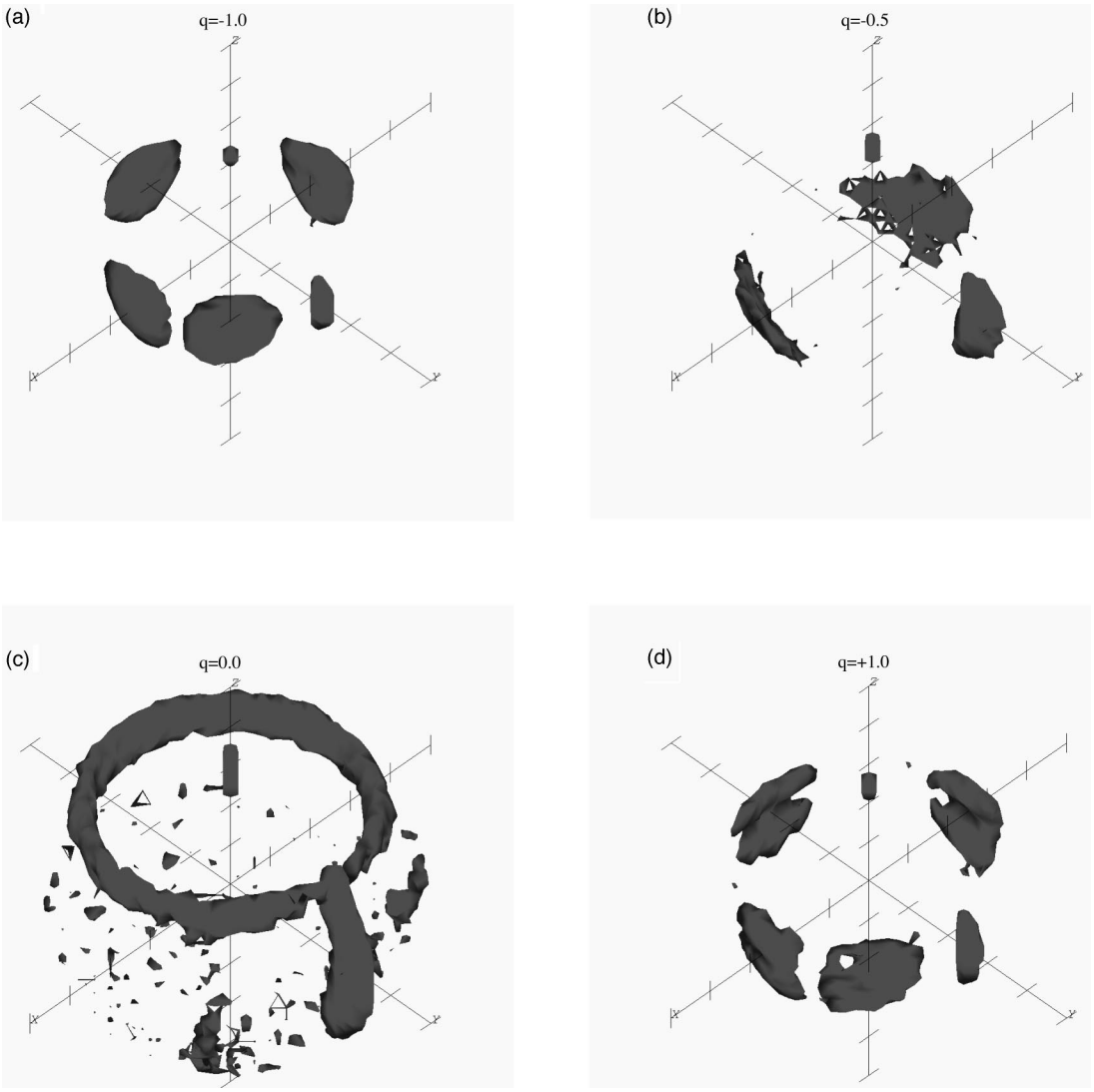

FIG. 6. The first solvation shell surrounding solutes of charge $q=-1,\ -0.5,\ 0$, and $+1$. The isodensity surfaces enclose regions with high probabilities of finding the center of mass of a water molecule. The isodensity surfaces surrounding the $q=-1,-0.5$, and $+1$ solutes correspond to a center of mass density equal to eight times the bulk density. The isodensity surfaces surrounding the $q=0$ solute correspond to four times the bulk density, and the ring (radius 2.5 Å) encircling the z axis lies in the $z=2$ Å plane. The marks on the axes are 1 Å apart. See the text for the definition of the coordinate systems.

ecules coordinate the solute roughly as if it was uncharged. The angular structure of the second solvation shell is, as expected, less pronounced than that of the first (see the discussion of the orientational contribution to the solvation entropy in Sec. V).

The coordination of water molecules around an ion depends on, among other things, the sign and size of its charge. It is clear from Fig. 2 that the $q=\pm 1$ and -0.5 solutes are surrounded by well defined first solvation shells. Integration over these shells to the first minima gives coordination numbers of 5.9 for the $q=\pm 1$ solutes and 4.0 for the $q=-0.5$ solute. This indicates that the $q=\pm 1$ solutes are octahedrally coordinated, whereas the $q=-0.5$ solute is tetrahedrally coordinated. We have looked further into how the water molecules are coordinated around the solutes using a local coordinate system attached to the molecules in the first solvation shell.

Let $\mathbf{r}_1$, $\mathbf{r}_2$, $\mathbf{r}_3$, and $\mathbf{r}_4$ denote the positions of the four closest coordinated molecules, ordered according to their distance from the solute ($\mathbf{r}_1$ is the closest), and let $\mathbf{r}_s$ denote the position of the solute. Further, let $\mathbf{r}_\perp=\mathbf{r}_i$ where $\mathbf{r}_i$ is selected among $\mathbf{r}_2$, $\mathbf{r}_3$, and $\mathbf{r}_4$ according to the criterion that $|(\mathbf{r}_i-\mathbf{r}_s)\cdot(\mathbf{r}_1-\mathbf{r}_s)|$ should be minimal. The coordinate axes are then defined by

$$\mathbf{e}_z=\frac{\mathbf{r}_1-\mathbf{r}_s}{|\mathbf{r}_1-\mathbf{r}_s|}, \tag{5a}$$

$$\mathbf{e}_y=\frac{\mathbf{r}_\perp-\mathbf{r}_\perp\cdot\mathbf{e}_z}{|\mathbf{r}_\perp-\mathbf{r}_\perp\cdot\mathbf{e}_z|}, \tag{5b}$$

$$\mathbf{e}_x=\mathbf{e}_y\times\mathbf{e}_z. \tag{5c}$$

In this coordinate system, the distribution of the mass centers of the water molecules has been calculated; see Figs. 6(a)–6(d). When investigating these distributions, the following picture of the coordination of water emerges: The solutes

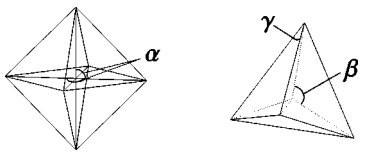

FIG. 7. The angles α, β, and γ used to estimate the deviations from octahedral and tetrahedral symmetry are indicated in the figure. Note that there are a number of angles equivalent to these that have been marked.

with charges $q=\pm 1$ are both, as expected, octahedrally coordinated [see Figs. 6(a) and 6(d)]. The octahedral coordination is the most pronounced for the negatively charged solute: The six maxima surrounding the negatively charged solute have higher peak values and are less dispersed. Further, the coordination deviates the least from perfect octahedral symmetry as discussed below. The $q=-0.5$ solute is tetrahedrally coordinated [see Fig. 6(b)]. One may note that although the coordination of the water molecules changes from octahedral to tetrahedral as q changes from -1 to -0.5, the most probable orientation of the water molecules remains unaffected; see Fig. 5.

The remaining solutes are surrounded by less well defined water structures, at least in the selected coordinate system. A ringlike maximum can be observed for the $q=0$ and $+0.2$ solutes [see Fig. 6(c)]. Tendencies toward the same type of ring formation can also be observed for the $q=-0.3$ and $+0.5$ solutes; however, the first solvation shell is considerably less structured. If the ringlike maximum indicates that the water molecules surrounding the solute form part of a relatively intact hydrogen-bond network; then it appears that either the $q=-0.3$ and $+0.5$ solutes disrupt the network to some extent, or have a less well defined position within the network.

The above shows that the coordination of water molecules around the $q=-1$, -0.5, and $+1$ solutes possesses either octahedral or tetrahedral features. In order to estimate the degree of deviation from these two types of perfect symmetries, we have considered (a) the deviations in the angles α, β, and γ indicated in Fig. 7; and (b) how well rotation of a perfect octahedron (or tetrahedron) can fit the center of mass points of the six (or four) closest coordinated water molecules.

Denote the angles obtained by joining two vertices of an octahedron via its center by α (see Fig. 7). For a perfect octahedron α can be either $\pi/2$ or π depending on the pair of vertices joined. In order to estimate the degree of octahedral symmetry in the first hydration shell, we have considered the angles formed between the mass centers of the water molecules in the first hydration shell via the solute. The root mean square diviation, $\Delta\alpha$, of these angles from π and $\pi/2$ has been estimated. Analogously, $\Delta\beta$ and $\Delta\gamma$ (see Fig. 7) have been used to estimate the degree of deviation from perfect tetrahedral symmetry. The average values of $\Delta\alpha$, $\Delta\beta$, and $\Delta\gamma$ have been calculated from the simulation; see Table II.

The second type of measure of the degree of deviation from perfect symmetry is defined by

$$d=\min_{\mathcal{R}}\sqrt{\frac{1}{n}\sum_{i=1}^{n}(\mathbf{r}_i-\mathbf{r}_i^o)^2}, \tag{6}$$

TABLE II. Deviations from octahedral and tetrahedral symmetry as quantified by angular and center of mass (com) deviations. $\Delta\alpha$, $\Delta\beta$, and $\Delta\gamma$ are the rms deviations of the angles defined in Fig. 7. r_{tet} and r_{oct} denote the average distance to the four and six closest water molecules, respectively. d and a measure how well an octahedron (or tetrahedron) can be fitted to the com points of the water molecules in the first coordination shell by rotation; see the text. The estimated standard deviation is less than one unit in the last digit in all cases.

	$q(e)$						
	-1.0	-0.5	-0.3	0.0	$+0.2$	$+0.5$	$+1.0$
$\Delta\alpha$	0.18	0.44	0.46	0.48	0.48	0.45	0.32
$\Delta\beta$	0.54	0.42	0.53	0.62	0.59	0.51	0.50
$\Delta\gamma$	0.28	0.25	0.33	0.42	0.40	0.32	0.28
r_{oct}	2.3	2.8	3.0	3.2	3.1	2.9	2.6
d_{oct}	0.15	0.49	0.51	0.56	0.54	0.48	0.29
a_{oct}	0.15	0.46	0.51	0.57	0.54	0.48	0.28
r_{tet}	2.3	2.5	2.8	3.0	3.0	2.8	2.5
d_{tet}	0.45	0.36	0.50	0.61	0.58	0.48	0.44
a_{tet}	0.46	0.36	0.50	0.63	0.59	0.48	0.44

where $\mathbf{r}_i$ is the position of the ith water molecule, and $\mathbf{r}_i^o$ is the position of the ith vertex of a perfect octahedron ($n=6$) or tetrahedron ($n=4$). Note that the radius of the octahedron (or tetrahedron) is set equal to the average distance of the six (four) closest coordinated water molecules. This average distance is also used as the length unit in Table II. The minimum is taken over the set of all possible rotations $\mathcal{R}$.

We have also estimated the angular part of the deviation from perfect geometry. It was obtained by first projecting the center of mass points $\mathbf{r}_i$ of the six (four) closest coordinated water molecules onto a unit sphere centered at the solute. Then the six (four) vertices of the octahedron (tetrahedron) were projected onto the same unit sphere. Finally, the distances a between the projections of the center of mass points and the projections of the vertices were measured along great circles on the sphere, the root mean square distance was calculated, and the minimum was taken over the set of all possible rotations $\mathcal{R}$; see Table II.

Clearly, the coordination shells surrounding the $q=\pm 1$ solutes deviate the least from octahedral symmetry. The angle α deviates on the average 0.18 and 0.32 from the corresponding values associated with perfect octahedral symmetry. Rotational fitting of an octahedron to the coordination shell also gives the smallest deviations in d_{oct} and a_{oct} for these solutes. The coordination shell surrounding the $q=-0.5$ solute deviates the least from tetrahedral symmetry as measured by the angles β and γ and the parameters d_{tet} and a_{tet}. The coordination shells surrounding the other solutes can neither be fitted to octahedral nor to tetrahedral symmetry. Further, one may note that a is close to d for all solutes, which reflects the fact that radial deformations of the coordination geometry are relatively small compared to angular deformations.

IV. HYDROGEN-BOND ARRANGEMENT

In addition to studying the spatial arrangement of the water molecules around the solute, we have studied how the

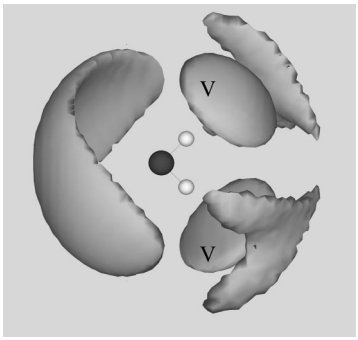

FIG. 8. The spatial distribution function $g_{OO}(\mathbf{r})$ used to define the hydrogen bond. The surfaces enclose volumes defined by Eq. (7) with $g_c=1.5$. The volumes marked by V grow slightly, but retain their shape, if g_c is lowered to 1.

topology of the hydrogen-bond network is affected by the solute. More specifically, we have looked at how the number and types of hydrogen bonds that a water molecule engages in depend on the distance from the solute. The methods used to analyze the network were introduced in Refs. [27–29], and applied to water-acetonitrile mixtures in Ref. [30].

We have used the effective hydrogen-bond definition to determine which pairs of water molecules are bonded. This definition is based on the spatial distribution function $g_{OO}(\mathbf{r})$, and its properties were discussed in Ref. [28]. For the present purposes we may view it as a geometric definition; that is, two water molecules are defined as bonded if their positions and orientations satisfy certain conditions. More precisely, one of the molecules must have its oxygen atom inside either of two volumes V located in the vicinity of the protons of the other molecule; see Fig. 8. The volumes [31] are defined by the relation

$$V=\{\mathbf{r}\,|\,g_{OO}(\mathbf{r})>g_c\}, \tag{7}$$

where $g_c=1$. Depending on the g_c selected, the number of bonded pairs of molecules changes. Previous investigations [28] indicate that $g_c=1$ is a reasonable choice: The average number of hydrogen bonds is relatively insensitive to changes in g_c around this value.

We will denote total number of hydrogen bonds that a water molecule is engaged in by n_t, the number of accepted protons by n_a, and the number of donated protons by n_d. Trivially the relation $n_t=n_a+n_d$ holds. The number of protons donated, n_d, can take the values 0, 1, or 2, and n_a can take the values 0, 1, 2, or 3. We will label the different *hydrogen-bond configurations* of a water molecule by n_dn_a and the probability to find a water molecule in a certain configuration will be denoted $p_{n_dn_a}$.

A natural starting point for the investigation of the hydrogen-bond network is the dependence of the average number of hydrogen bonds per water molecule, n_t, on the distance from the solute; see Fig. 9(c). Close to the solute the number of bonds decreases below 1.6, and at large distances it tends towards the bulk value 3.338 ± 0.0015. Between these limits, the average number of bonds varies differently depending on the charge of the solute: for solutes with charges -1, -0.5, and $+1$ there are significant oscillations, whereas variations are less pronounced for the other solutes.

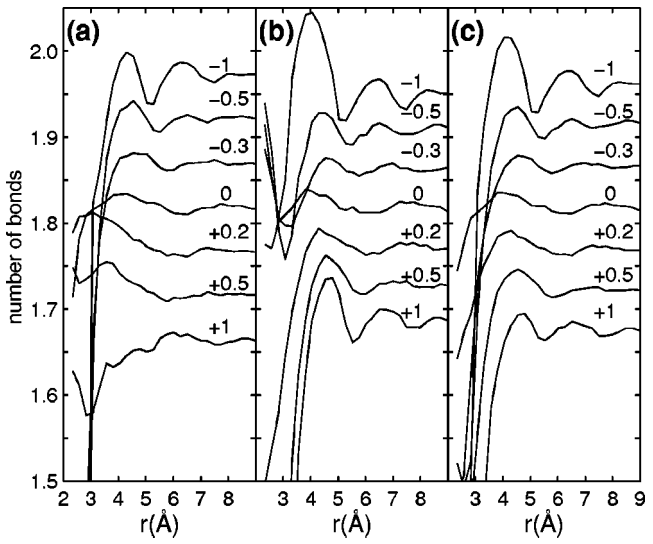

FIG. 9. The average numbers of bonds that a water molecule engages in as a function of the distance r from the solute. (a) Number of bonds donated, n_d. (b) Number of bonds accepted, n_a. (c) Total number of bonds n_t, divided by 2. The curves corresponding to the $q=+1$, $+0.5$, $+0.2$, 0, -0.3, -0.5, and -1 solutes have been displaced by 0, 0.1, 0.2, 0.3, 0.4, 0.5, and 0.6 units, respectively.

The total number of hydrogen bonds among the water molecules surrounding the solute, minus the total number of hydrogen-bonds in the pure water system are listed in Table III. One may note that the total number of hydrogen bonds decreases when a solute is inserted, except in the case of the $q=+0.2$ for which it remains unchanged. The decrease is the largest for the $q=-1.0$ and -0.5 solutes, for which the number of bonds decreases by 4.6 and 2.7, respectively. A significant part of the decrease in the total number of hydrogen-bonds is due to a loss of hydrogen bonds among the water molecules in the first solvation shell; see Table III. The contribution from water molecules outside the first solvation shell is less than 2 for all solutes. One should however note that the sign of the contribution varies: There is a net decrease in the number of hydrogen bonds of 1.7 for the $q=-1$ solute, whereas there is a net increase of 1.5 for the $q=+1$ solute. Moreover, if one regards solutes that are surrounded by well defined hydration shells (that is the $q=-1$, -0.5, and $+1$ solutes) as bonded to the water molecules in the first hydration shell, then the total number of

TABLE III. The change in the number of hydrogen bonds among the water molecules due to the insertion of the solutes. Δ_t denotes the total number of hydrogen bonds among the water molecules surrounding the solute minus the total number of hydrogen bonds in the bulk simulation. Δ_1 denotes the number of hydrogen bonds among the water molecules in the first solvation shell minus the number of hydrogen bonds that the same number of water molecules form in the bulk simulation. The estimated standard deviations are less than 0.3 for Δ_t, and less than 0.03 for Δ_1.

$q(e)$	-1.0	-0.5	-0.3	0.0	0.2	$+0.5$	$+1.0$
Δ_t	-4.6	-2.7	-1.8	-0.1	0.0	-0.2	-2.1
Δ_1	-2.9	-1.7	-1.3	$+0.1$	-0.1	-1.3	-3.6

TABLE IV. The average number of bonds, n_t, the average number of bonds accepted, n_a, and the average number of bonds donated, n_d, for water molecules in the first hydration shell at a distance r from the solute. q denotes the charge of the solute. The estimated standard deviation is less than half a unit in the last digit.

$q(e)$	r (Å)	n_t	n_a	n_d
−1.0	2.3	2.4	1.6	0.7
−0.5	2.4	2.5	1.7	0.9
−0.3	2.6	2.6	1.7	1.0
0.0	3.0	3.3	1.7	1.7
+0.2	2.9	3.2	1.5	1.7
+0.5	2.6	2.7	1.0	1.7
+1.0	2.5	2.1	0.5	1.6

bonds in these systems increases by 1.4, 1.3, and 3.9, respectively.

A more detailed picture of the hydrogen-bond structure is obtained by studying how n_d and n_a vary. In the first solvation shell the water molecules can bond directly to the solute. Naturally, this reduces n_d or n_a depending on the sign of the solute's charge (see Table IV). Further, one can expect this effect to increase with the size of the charge $|q|$, as is also observed: n_d is about 1.7 for positively charged solutes and about 0.9 for negatively charged solutes, whereas n_a is about 1.7 for negatively charged solutes and ranges from 1.5 to 0.5 for positively charged solutes.

In bulk water, n_a and n_d are both equal to about 1.7. The four water molecules in the vicinity of the $q=+0.5$ solute have $n_a=1.0$, which indicates that together they have lost about three hydrogen bonds. Previous considerations of the spatial arrangement of the water molecules in the vicinity of this solute gave that the solute acts as a double proton donor (see Sec. III). Thus the system regains about two of the three hydrogen bonds lost. Analogously, the system regains about two of the three hydrogen bonds lost among the water molecules surrounding the $q=-0.3$ solute.

The dependence of n_a and n_d on the distance r from the solute are shown in Fig. 9. One can note that n_d varies moderately with r for the solutes with $q \geqslant 0$. For the other solutes, the variations in n_d are confined mainly to the first shell, the exception being the $q=-1$ solute for which oscillations persist up to about $r=6$ Å. The value of n_a depends more strongly on the distance from the solute than does n_d: There are pronounced oscillations beyond the first solvation shell for solutes of charge -1, -0.5, and $+1$. It is not clear to us why n_a fluctuates more than n_d for the $q=+1$ solute.

Further insight into the structure of the hydrogen-bond network has been obtained by considering the probabilities of the different hydrogen-bond configurations in the first and second solvation shells; see Table V. When estimating these

TABLE V. The probabilities that water molecules in the first and second hydration shells have certain hydrogen-bond configurations. The shells are defined by maxima in the radial distribution functions, see the text. The charge of the solute is denoted by q and the distance from the solute to the maximum by r. The probabilities for the different hydrogen-bond configurations are indicated by $p_{n_d n_a}$, where n_d denotes the number of hydrogen bonds that the water molecule participates in as a proton donor, and n_a the number of hydrogen bonds that it participates in as an acceptor. For comparison, results are included for bulk water and for shells with $r=4.3$ Å. The probabilities for bulk water are also given. The estimated standard deviation is less than three units in the last digit in all cases. It is also less than 20% in all cases except those marked by a.

		Configuration probability											
q (e)	r (Å)	p_{00}	p_{10}	p_{20}	p_{01}	p_{11}	p_{21}	p_{02}	p_{12}	p_{22}	p_{03}	p_{13}	p_{23}
−1.0	2.3	0.006	0.013	0.000	0.108	0.27	0.000	0.137	0.44	0.000	0.005	0.023	0.000
−0.5	2.4	0.003	0.012	0.000	0.062	0.27	0.002[a]	0.083	0.52	0.003[a]	0.004	0.046	0.000
−0.3	2.6	0.003	0.013	0.002	0.060	0.26	0.04	0.076	0.44	0.06	0.004	0.033	0.006
0.0	3.0	0.001	0.006	0.009	0.013	0.11	0.22	0.013	0.15	0.43	0.000	0.006	0.032
+0.2	2.9	0.001	0.008	0.015	0.015	0.13	0.31	0.007	0.10	0.39	0.000	0.003	0.016
+0.5	2.6	0.005	0.038	0.075	0.019	0.20	0.52	0.002	0.030	0.11	0.000	0.000	0.002[a]
+1.0	2.5	0.025	0.178	0.319	0.013	0.13	0.32	0.000	0.003	0.008	0.000	0.000	0.000
−1.0	4.2	0.000	0.005	0.010	0.008	0.089	0.21	0.013	0.15	0.45	0.001	0.012	0.053
−0.5	4.3	0.001	0.005	0.010	0.013	0.101	0.22	0.013	0.15	0.45	0.000	0.007	0.035
0.0	4.8	0.001	0.006	0.010	0.013	0.11	0.22	0.013	0.15	0.44	0.000	0.008	0.038
+0.2	4.8	0.001	0.006	0.011	0.012	0.10	0.21	0.013	0.15	0.44	0.000	0.008	0.039
+1.0	4.6	0.001	0.005	0.007	0.013	0.097	0.19	0.017	0.17	0.44	0.001	0.011	0.046
−0.3	4.3	0.001	0.006	0.010	0.013	0.11	0.22	0.014	0.15	0.44	0.000	0.007	0.036
0.0	4.3	0.001	0.005	0.010	0.012	0.10	0.22	0.013	0.15	0.44	0.000	0.008	0.038
+0.2	4.3	0.001	0.005	0.010	0.012	0.097	0.21	0.013	0.15	0.45	0.000	0.007	0.039
+0.5	4.3	0.001	0.005	0.010	0.011	0.099	0.21	0.014	0.15	0.45	0.000	0.009	0.041
bulk		0.001	0.006	0.011	0.014	0.107	0.22	0.014	0.15	0.43	0.000	0.008	0.036

[a]The estimated standard deviation is less than 25%.

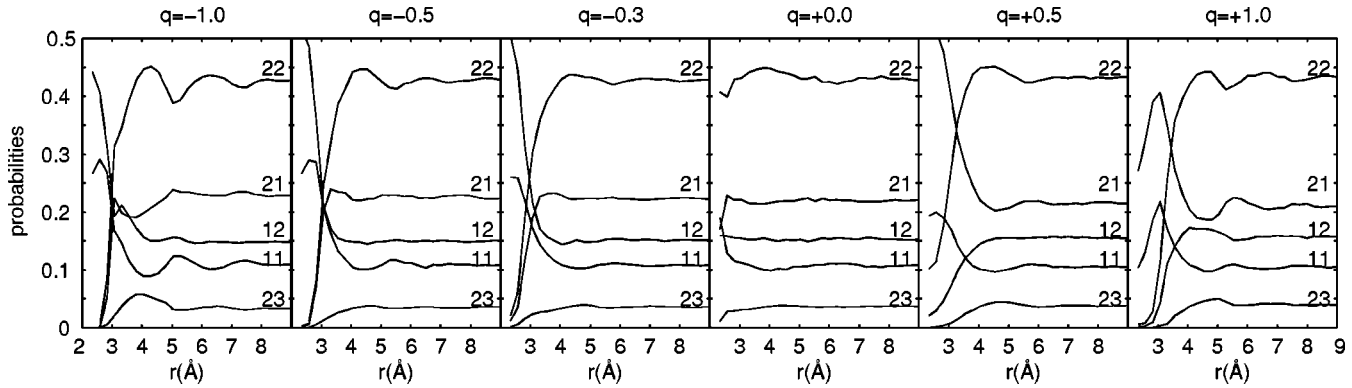

FIG. 10. The probabilities $p_{n_d n_a}$ describing the fraction of water molecules in different hydrogen-bond configurations are plotted as functions of the distance r between the solute and the water molecule. The curves are marked by $n_d n_a$, where n_d and n_a denote the number of hydrogen bonds donated and accepted, respectively. Note that the lower-probability hydrogen-bond configurations have been omitted.

probabilities, the solvation shells have been defined as the 0.25-Å-thick spherical shells centered on the maxima of the solute-oxygen radial distribution functions (compare Fig. 2).

In the first solvation shell, the 12 configuration (that is, $n_d=1$ and $n_a=2$) is the most probable for solutes with $q<0$, whereas the 21 configuration is the most probable for solutes with $q>0.2$. Further, the 11 configuration is the second most probable configuration for solutes with $|q|>0.2$. Considering the $q=+0.5$ and -0.3 solutes, we may note that the former corresponds to a maximum in p_{21}, and the latter has a relatively high value of p_{12}.

The first solvation shell surrounding the $q=0$ solute has a bond structure resembling that of bulk water. The different hydrogen-bond configurations of the water molecules in this shell all have probabilities $p_{n_d n_a}$ comparable to those of the same configurations in bulk water. In particular, one may note that p_{22} is equal to 0.43, which is the same as in bulk water. The first solvation shell surrounding the $q=+0.2$ solute has a bond structure that differ significantly from that of bulk water. Nevertheless, these differences are small in comparison with the differences in the configuration probabilities induced by the more highly charged solutes.

Turning to the $q=-0.3$ and the $+0.5$ solutes, we note that the probability of the 22 configuration is reduced from the bulk value of 0.43 to 0.06 and 0.11 for the $q=-0.3$ and $+0.5$ solutes, respectively. On the other hand, the probability of the 12 configuration is enhanced for the $q=-0.3$ solute, and the probability of the 21 configuration is enhanced for the $q=+0.5$ solute. Further, about two of the four water molecules in the first hydration shell of these solutes coordinate tetrahedrally to the solute. Thus, in addition to the 22 coordinated water molecules, there is a number of water molecules that are coordinated in a ''22-like'' manner.

The $q=-1$, -0.5, 0, $+0.2$, and $+1$ solutes all exhibit second solvation shells in terms of a second maximum in $g_{\mathrm{SO}}(r)$. For the water molecules in these shells, the different hydrogen-bond configurations occur with frequencies similar to those in bulk water. However, there are some differences: the 23 configuration has a higher probability in these shells than in bulk water (except for the $q=-0.5$ solute). Moreover, for the $q=+1$ solute, the probabilities of the 12, 13, and 22 configurations are also enhanced, and, for the $q=-1$ solute, the probabilities of the 13 and 22 configurations are enhanced. Further, the density maxima of the second solvation shells of the $q=-1$, -0.5, and $+1$ solutes coincide with maxima in n_a and n_t; see Fig. 9. Some of the probabilities $p_{n_d n_a}$ also take extreme values in these shells; see Fig. 10.

Since the $q=-0.3$ and $+0.5$ solutes correspond to maxima in the solvation entropy, and since they are associated with the disappearance of the second maxima in $g_{\mathrm{SO}}(r)$, one might expect the hydrogen-bond network surrounding these molecules to be perturbed in some sense (compare Lynden-Bell and Rasaiah [4]). Further, if such perturbations prevail, then it is reasonable to expect traces of them to be visible in the probability distributions describing the frequency with which the various hydrogen-bond configurations occur. The probability distributions of the water molecules at $r=4.3$ Å distance from the solute are given in Table V. The differences are small between the distributions describing the hydrogen-bond configurations surrounding, on the one hand, the $q=0$ and $+0.2$ solutes and, on the other hand, the $q=-0.3$ and $+0.5$ solutes. Further, all configurations occur roughly as frequently as in bulk water. Also at distances larger than $r=4.3$ Å from these four solutes, the situation closely resembles that of bulk water (compare Figs. 9 and 10). Thus the disappearance of the second maximum in $g_{\mathrm{SO}}(r)$ for the $q=-0.3$ and $+0.5$ solutes does not appear to be associated with any major change in the topology of the hydrogen-bond network outside the first hydration shell.

V. SOLVATION ENTROPY

So far, we have compared spatial and topological aspects of the solvation structures surrounding solutes of different charges. We have been particularly interested in differences in the solvation structures surrounding solutes corresponding to extrema in the solvation entropy. In order to clarify the relation between the solvation structure and the solvation entropy, we have calculated the solute-water two-body contribution to the solvation entropy. Below we first define this two-body contribution and then we consider the results for different solutes.

The solvation entropy can be defined as

$$\Delta S = S_{\mathrm{mixture}} - S_{\mathrm{water}} - S_{\mathrm{solute}}, \tag{8}$$

where S_{solute} denotes the entropy of a single solute in an ideal gas phase, S_{water} the entropy of the pure water system, and

S_{mixture} the entropy of the mixture. In the canonical ensemble each of these terms is given by an expression of the type

$$S = -\frac{k}{N!h^s}\int \rho(p,q)\ln\rho(p,q)dpdq, \tag{9}$$

where N is the number of particles (or molecules), s is the number of degrees of freedom of the system, h is the Planck constant, and k is the Boltzmann constant. The system's kinetic and configurational degrees of freedom are denoted by p and q, respectively, and $\rho(p,q)$ is the N-particle distribution function. Integral (9) above can be solved analytically for the solute term, giving

$$S_{\text{solute}} = k\left(\frac{3}{2} - \ln(\rho_s\Lambda^3)\right), \tag{10}$$

where ρ_s is the number density of the solute and Λ is the de Broglie wavelength. The integral can however not be solved analytically for the water and mixture terms; but, using a Kirkwood-type factorization [16] of the N-particle distribution function, one can rewrite S_{water} and S_{mixture} as sums over the partial n-body distribution functions [17,32]. Doing this, one obtains the following expansion of the solvation entropy,

$$\Delta S = S_{\text{sw}}^{(2)} + \Delta S_{\text{ww}}^{(2)} + S_{\text{sww}}^{(3)} + \Delta S_{\text{www}}^{(3)} + \cdots, \tag{11}$$

where

$$S_{\text{sw}}^{(2)} = -kN_w\rho_s\int g_{\text{sw}}^{(2)}\ln g_{\text{sw}}^{(2)}d\mathbf{r} + kN_w\rho_s\int (g_{\text{sw}}^{(2)}-1)d\mathbf{r} \tag{12a}$$

and

$$S_{\text{ww}}^{(2)} = -kN_w\frac{\rho_w}{2\Omega}\int g_{\text{ww}}^{(2)}\ln g_{\text{ww}}^{(2)}\, d\mathbf{r}\, d\boldsymbol{\omega} + kN_w\frac{\rho_w}{2\Omega}\int (g_{\text{ww}}^{(2)}-1)d\mathbf{r}\, d\boldsymbol{\omega}. \tag{12b}$$

Above, ρ_s denotes the number density of the solute, ρ_w the number density of the water molecules, $g_{\text{ww}}^{(2)}$ the two-body water-water distribution function, and $g_{\text{sw}}^{(2)}$ the two-body solute-water distribution function. Further, $\mathbf{r}$ is the position of a molecule, $\boldsymbol{\omega}$ is the Euler angles describing its orientation, and Ω is $8\pi^2$. N_w is the number of water molecules (that is 255 in our simulations), and k is Boltzmann's constant. The second term in expansion (11) is the difference between $S_{\text{ww}}^{(2)}$ obtained from the mixture and the pure water system, respectively. This difference need not tend to zero as N_w tends to infinity. In fact, the following will show that it is reasonable to expect it to be of the same order of magnitude as $S_{\text{sw}}^{(2)}$ (cf. Ref. [33]). We have calculated $S_{\text{sw}}^{(2)}$ from our MD simulations. The other terms in Eq. (11) were inaccessible because of the computational resources required.

The full solvation entropy varies bimodally with q, in contrast to $S_{\text{sw}}^{(2)}$ which has a single maximum at $q=0$; see Fig. 1. The difference between ΔS and $S_{\text{sw}}^{(2)}$ is due to $\Delta S_{\text{ww}}^{(2)}$, and other higher order terms in the expansion (11). Further, $S_{\text{sw}}^{(2)}$ is less than ΔS for all except the $q=0$ and $+0.2$ solutes, for which the converse is true. In this sense one may thus say that the $q=0$ and $+0.2$ solutes enhance the water structure, whereas the other solutes disrupt it. Moreover, as the solute's charge (that is $|q|$) increases, the difference between $S_{\text{sw}}^{(2)}$ and ΔS becomes larger. The solute-water correlations thus increase, whereas the water-water correlations decrease. One may also note that ΔS is negative for all q, which is expected considering excluded volume effects.

The two-body contribution to the solvation entropy can be separated into an orientational $S_{\text{sw},o}^{(2)}$ and a radial or nonorientational part $S_{\text{sw},r}^{(2)}$ by writing $g_{\text{sw}}^{(2)}$ as a product,

$$g_{\text{sw}}^{(2)} = g(r)a(r,\theta,\phi), \tag{13}$$

of the radial distribution function $g(r)$ and a function $a(r,\theta,\phi)$ describing the orientation of the water molecules [18,32]. The angles θ and ϕ are defined in Fig. 4. Inserting this factorization of $g_{\text{sw}}^{(2)}$ into expression (12a) for $S_{\text{sw}}^{(2)}$, we thus obtain

$$S_{\text{sw}}^{(2)} = S_{\text{sw},o}^{(2)} + S_{\text{sw},r}^{(2)}, \tag{14}$$

where

$$S_{\text{sw},r}^{(2)}/kN_{\text{w}} = -\rho_s\int_0^\infty dr\, 4\pi r^2 g(r)\ln g(r) - \rho_s\int_0^\infty dr\, 4\pi r^2(g(r)-1) \tag{15}$$

and

$$S_{\text{sw},o}^{(2)}/kN_w = -\rho_s\int_0^\infty dr\, 4\pi r^2 g(r)\frac{1}{4\pi}\int_0^\pi\int_0^{2\pi} \times d\theta\sin\theta\, d\phi\, a(r,\theta,\phi)\ln a(r,\theta,\phi). \tag{16}$$

The radial part $S_{\text{sw},r}^{(2)}$, would hence be equal to $S_{\text{sw}}^{(2)}$ if the solvent lacked orientational degrees of freedom. Further, provided that the solute did not induce any orientational order among the water molecules, then $a\equiv 1$ and $S_{\text{sw},o}^{(2)}$ would become maximal that is it would become zero and again $S_{\text{sw},r}^{(2)}$ would be equal to $S_{\text{sw}}^{(2)}$. The radial and orientational parts of the two-body entropy are given in Table VI. One can note that the orientational part varies approximately parabolically with q, whereas the radial part has the characteristic bimodal form of the full solvation entropy with maxima at $q=-0.3$ and $+0.5$. Further, for all except the $q=0$ and $+0.2$ solutes, $S_{\text{sw}}^{(2)}$ is dominated by the orientational part.

One can break down the orientational and radial contributions to $S_{\text{sw}}^{(2)}$ into contributions from different spherical shells surrounding the solute. The orientational part can, for example, be viewed as a sum of contributions,

$$dS = -\rho_s dr\, 4\pi r^2 g(r)\frac{1}{4\pi}\int_0^\pi\int_0^{2\pi} \times d\theta\sin\theta\, d\phi\, a(r,\theta,\phi)\ln a(r,\theta,\phi), \tag{17}$$

from shells of thickness dr. In this expression dS may be viewed as entropy due to the orientational freedom of a water molecule at distance r multiplied by the average number of

TABLE VI. Different contributions to the solvation entropy in units of Boltzmann's constant k. $S^{(2)}_{sw,r}$ denotes the radial, $S^{(2)}_{sw,o}$ the orientational, and $S^{(2)}_{sw}$ the total two-body solute-water solvation entropy. S_{LBR} denotes the solvation entropy read from Fig. 5 in Ref. [4]. S_{BLL} denotes the solvation entropy obtained from our expanded ensemble simulation. We have set S_{BLL} equal to S_{LBR} at $q=0$; see Sec. II. $S^{(2)}_{sw}$, $S^{(2)}_{sw,o}$, and $S^{(2)}_{sw,r}$ have been corrected for the systematical error due to noise; see Sec. V. The standard deviation in S_{BLL} has been estimated by partitioning the simulation in ten parts.

	$q(e)$						
	-1.0	-0.5	-0.3	0.0	$+0.2$	$+0.5$	$+1.0$
$S^{(2)}_{sw,r}$	-12.8	-4.4	-2.0	-3.2	-2.9	-2.9	-7.5
$S^{(2)}_{sw,o}$	-30.7	-11.6	-4.4	-3.0	-3.3	-4.3	-12.0
$S^{(2)}_{sw}$	-43.6	-16.0	-6.4	-6.1	-6.3	-7.2	-19.5
S_{LBR}	-28	-8	-2	-7	-8	-5	-10
S_{BLL}	-32.7 ± 1.9	-11.4 ± 1.4	-5.8 ± 1.0	-7	-9.0 ± 0.8	-7.2 ± 1.1	-14.3 ± 1.1
$S_{LBR}-S^{(2)}_{sw}$	$+15.6$	$+8.0$	$+4.4$	-0.9	-1.7	$+2.2$	$+9.5$
$S_{BLL}-S^{(2)}_{sw}$	$+10.9$	$+4.6$	$+0.6$	-0.9	-2.7	-0.0	$+5.2$

water molecules at this distance. However, it is not clear to us what the analogous decomposition of the radial part would mean: There are different contributions from different shells to integral (15), but it is meaningless to say that a region of high density contributes more or less to the entropy than a region of low density. The existence of one presupposes the existence of the other. For the same reasons, it appears better to speak about the orientational entropy relative to the solute associated with one water molecule in a certain solvation shell, than about the total orientational contribution from a certain shell, since the latter will be dependent on the local density of water molecules in different shells. The orientational entropies of water molecules in the first and second solvation shells, and in a spherical shell with $r=4.3$ Å, are listed in Table VII.

In order to estimate the accuracy in our determination of $S^{(2)}_{sw}$, several sources of error must be considered. First, the noise in our estimate of the distribution function $g^{(2)}_{sw}$ gives rise to a systematical error and a statistical error. These errors were estimated by partitioning the simulation time in intervals of different length (10×0.2, 5×0.4, and 1×2 ns). For each of these intervals $S^{(2)}_{sw}$ was calculated via Eq. (12a). The mean value and the standard deviation in $S^{(2)}_{sw}$ were then estimated for each partition. The systematical error due to the noise was estimated as the difference between the mean value of the entropy obtained from the 5×0.4-ns partition and the entropy obtained from 1×2-ns partition (see Table VIII). We expect this estimate to provide an upper bound of the systematical error due to the noise. The statistical error was estimated using the standard deviation obtained for the 5×0.4-ns partition (see Table VIII).

Moreover, in order to evaluate the integrals in Eq. (12a), the solute-water configuration space was partitioned into volumes dV. We have used two different partitions in order to estimate the error due to the fact that g_{sw} is not constant on the dV. The first partition has

$$dV = dr \times d\cos\theta \times d\phi, \tag{18}$$

where $dr=0.2$, $d\cos\theta=2/30$, and $d\phi=\pi/30$, and the second, finer, partition has $dr=0.1$, $d\cos\theta=2/60$, and $d\phi=\pi/60$. The difference between the results obtained using the two partitions of the configuration space is listed in Table VIII. We estimate that 0.2 k of this difference is due the different systematical errors caused by the noise, and the rest is due to the difference in resolution between the partitions.

TABLE VII. Contributions dS to the orientational entropy from spherical shells of different radii r centered on the solute. The shells are 0.3 Å thick. The radii have been selected so that the shells coincide with the maxima of the first and second solvation shells (cf. Fig. 2). The shells at $r=4.3$ Å were also considered. dS is defined by Eq. (17) and $dS_{one}=dS/n$, where n is the average number of water molecules in the shell. The entropy is in units of Boltzmann's constant k and the radii are in Å. The statistical errors are less than 1% in first solvation shells and less than 4% in the other.

	$q(e)$						
	-1.0	-0.5	-0.3	0.0	$+0.2$	$+0.5$	$+1.0$
r	2.3	2.4	2.6	3.0	2.9	2.6	2.5
dS	-20.2	-6.90	-2.27	-0.55	-0.78	-1.25	-5.73
dS_{one}	-3.90	-2.88	-1.45	-0.27	-0.43	-0.82	-1.59
r	4.2	4.3		4.8	4.8		4.6
dS	-1.18	-0.18		-0.07	-0.07		-0.56
dS_{one}	-0.31	-0.06		-0.03	-0.03		-0.16
r	4.3	4.3	4.3	4.3	4.3	4.3	4.3
dS	-1.35	-0.18	-0.13	-0.19	-0.17	-0.09	-0.24
dS_{one}	-0.33	-0.06	-0.05	-0.10	-0.08	-0.04	-0.09

TABLE VIII. Different errors in $S^{(2)}_{sw}$ in units of k. The statistical and systematical errors due to noise in $g^{(2)}_{sw}$ are denoted $S_{noise,stat}$ and $S_{noise,syst}$, respectively. The difference between $S^{(2)}_{sw}$ as calculated using the finer and the grosser partition of the solute-water configuration space is denoted by $S_{resol,syst}$.

	$q(e)$						
	-1.0	-0.5	-0.3	0.0	$+0.2$	$+0.5$	$+1.0$
$S_{noise,stat}$	0.05	0.03	0.04	0.05	0.05	0.02	0.09
$S_{noise,syst}$	0.24	0.24	0.24	0.24	0.24	0.24	0.24
$S_{resol,syst}$	1.40	0.64	0.34	0.26	0.27	0.32	0.63

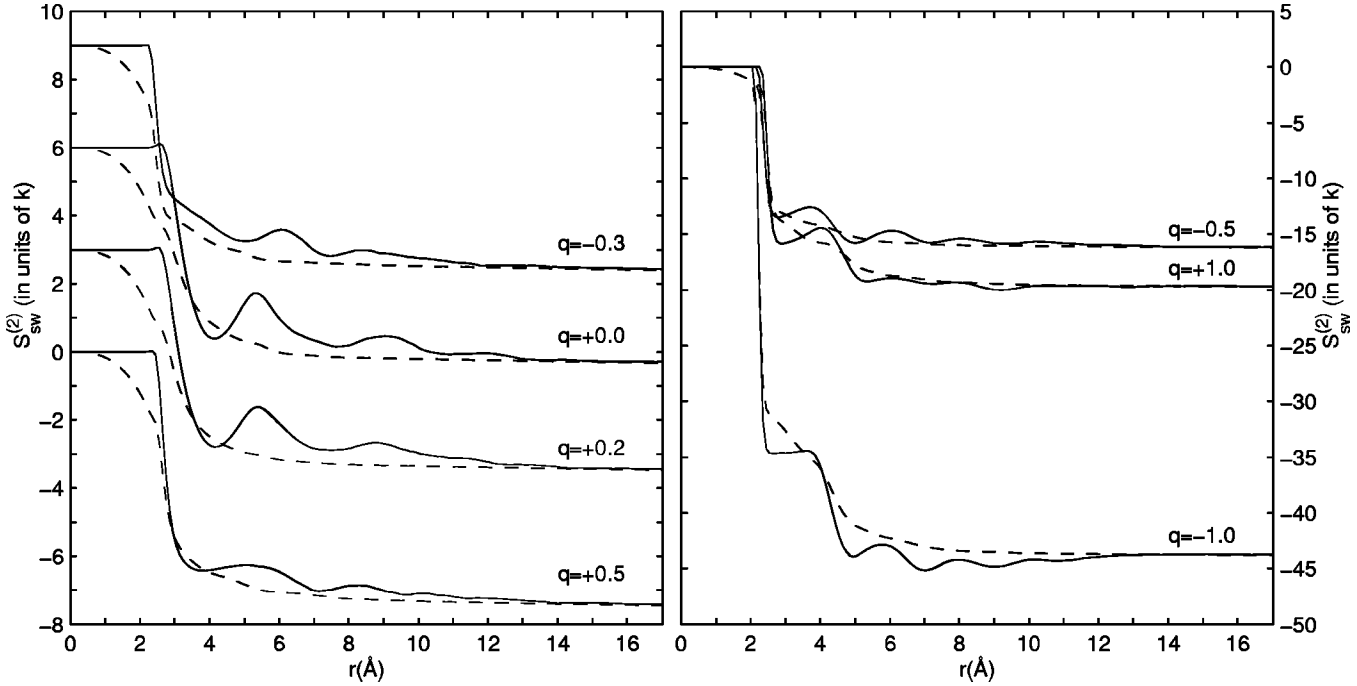

FIG. 11. The two-body solute-water contribution $S_{sw}^{(2)}$ to the solvation entropy. The integrals in Eq. (12a) have been carried out over spheres of radii r centered on the solute. The dashed curves have been obtained using the local form of the solvation entropy [i.e., both terms in Eq. (12a)] and the solid curves have been obtained using the nonlocal form [i.e., the first term in Eq. (12a)]. Note that the curves corresponding to the $q=+0.2$, $+0.0$, and -0.3 solutes have been displaced by $3k$, $6k$, and $9k$, respectively.

We assume that the error due to the finite resolution of the finer partition is less than the difference between the results obtained from the finer and grosser partitions, respectively. The error caused by insufficient resolution is mainly due to the fine structure in the first hydration shell, and it increases with $|q|$ since the more highly charged solutes are more strongly correlated with the surrounding water molecules.

Considering the different errors in Table VIII, we conclude that the statistical error due to the noise is less than 0.1 k for all solutes. The systematical error due to the noise decreases the solvation entropy by about 0.2 k (not more than 0.24 k). The error due to the finite resolution of the finer partition depends on the solute's charge; it ranges from about 1.2 k for the $q=-1$ solute to about 0.06 k for the uncharged solute.

One should also consider the possibility that the relatively small volume of our simulation cell may influence our estimate of the solvation entropy. We have evaluated the integrals in Eq. (12a) over the full simulation cell. This would be necessary if the nonlocal form of the solvation entropy [34] was used, and it is still preferable when using the local form of the solvation entropy [17] as we have. The reason that it is preferable is that contributions to the integrals in Eq. (12a) decay relatively slowly with the distance from the solute. In Fig. 11 the integrals in Eq. (12a) have been evaluated for spheres of increasing radius r centered on the solute. It is clear that the local form of the solvation entropy converges faster than the nonlocal form. At $r=L/2$ the local form deviates less than 0.2 k from the value obtained when the integral is evaluated over the full volume.

VI. LIFETIMES

We have calculated the average time τ that water molecules spend inside spheres of different radii centered on the solute; see Table IX. More precisely, we have only considered water molecules that spend at least 2 ps inside a given sphere when calculating the averages. The average lifetime does not include the 2-ps-long time period necessary for the molecule to be considered. This definition has the advantage that only water molecules that have properly entered a given sphere will be considered when estimating the average time. Molecules at the boundary that have rapidly in and out of the sphere are thus not considered. In the following we will usethe term *lifetime* for the average time spent inside a

TABLE IX. The average time (in ps) spent by a water molecule inside spheres of different radii (in Å) centered on the solute. r_i denotes the radius of a sphere enclosing on the average i water molecules. τ_i denotes the average time that water molecules spend inside this sphere; see the text for an exact definition. The estimated standard deviation is less than two units in the last digit in all cases except where other is indicated. q denotes the charge of the solute.

	$q(e)$						
	-1.0	-0.5	-0.3	0.0	$+0.2$	$+0.5$	$+1.0$
r_4	2.4	3.0	3.2	3.3	3.3	3.1	2.6
r_6	3.5	3.8	3.6	3.5	3.5	3.5	3.4
r_{20}	4.9	5.2	5.3	5.4	5.4	5.3	5.1
r_{30}	5.9	6.1	6.1	6.1	6.1	6.1	6.0
τ_4	–[a]	9.6	3.6	4.2	4.0	4.0	21
τ_6	41[b]	6.5	4.1	4.8	4.6	4.8	19
τ_{20}	17	10	6.6	7.1	7.0	7.6	12
τ_{30}	14	11	7.5	7.9	7.7	8.5	13

[a]The exchange is so slow that we cannot estimate the lifetime in this case.

[b]The estimated standard deviation is 4 in this case.

sphere of a given radius.

Looking at Table IX, one may first note that the more highly charged solutes contract the water structure surrounding them. Thus the radius of a sphere containing a fixed number of water molecules decreases as the magnitude of the charge increases. Further, there is a general trend for the lifetimes to increase with the magnitude of the solute's charge, which is equivalent to a slow down of the exchange of water molecules surrounding the solute with water molecules in the bulk. The $q=-0.3$ solute provides an exception: it is associated with shorter lifetimes than both the $q=-0.5$ and 0 solutes. As the $q=-0.3$ solute is associated with a maximum in the solvation entropy, this is perhaps not unexpected. The $q=+0.5$ solute is also associated with a maximum in the solvation entropy, but in this case we observe no minimum in the lifetimes. However, for the smaller spheres (r_4 and r_6) one may note that the lifetimes are comparable to those obtained for the $q=0$ and $+0.2$ solutes.

The $q=\pm 1$ solutes are surrounded by well defined octahedral solvation shells, and the $q=-0.5$ solute by a well defined tetrahedral solvation shell; see Fig. 6. The average times spent inside spheres of radii r_4 and r_6 reflect how strongly the solute bonds the water molecules in these solvation shells. The $q=-1$ solute bonds the water molecules the strongest, the $q=+1$ solute the second strongest, and the $q=-0.5$ solute the weakest. One may also note that τ_6 is significantly smaller than τ_4 for the $q=-0.5$ solute, whereas they are almost equal for the $q=+1$ solute. This reflects the fact that the former of these solutes is tetrahedrally coordinated, whereas the latter is octahedrally coordinated.

VII. CONCLUSION

We have begun our analysis by considering how closely our simulation conditions can be thought to mimic infinite dilution. The electric field in the simple cubic Wigner solid used in the simulations was found to be sufficiently similar to that surrounding an isolated point charge. By sufficiently similar we mean that one can expect the hydration structures surrounding solutes at infinite dilution to agree well with those obtained from our simulations. The agreement between our results and those obtained by Lynden-Bell and Rasaiah [4] for a smaller fcc system also supports this conclusion.

When an ion is inserted into water, it disrupts the hydrogen-bond network in its vicinity and creates one or several coordination shells. This is what we have observed for the $q=-1$, -0.5, and $+1$ solutes. Insertion of a noble gas atom, on the other hand, is not thought to disrupt, but rather to enhance the water-water correlations. We have calculated the solute-water two-body contribution $S_{\mathrm{sw}}^{(2)}$ as well as the solvation entropy S. The two-body contribution is larger than the solvation entropy for the $q=0$ and $+0.2$ solutes, which indicates that the water-water correlations are enhanced by these solutes. For the more highly charged solutes the converse is observed, that is $S_{\mathrm{sw}}^{(2)}$ is less than S, which indicates that the water-water correlations are reduced.

The topology of the hydrogen-bond network in the first solvation shell differs from that of pure water for all solutes studied, although the differences are small for the $q=0$ solute. Beyond the first solvation shell, the topology of the hydrogen-bond network closely resembles that of bulk water for the solutes with charges -0.3, 0, $+0.2$, and $+0.5$. In particular, one may note that outside the first solvation shell we find no significant differences between the topology of the hydrogen-bond network surrounding the $q=-0.3$ and $+0.5$ solutes on the one hand, and the $q=0$ and $+0.2$ solutes on the other hand. The remaining more highly charged solutes (that is, the $q=\pm 1$ and $+0.5$ solutes) also perturb the topology outside the first solvation shell. Nevertheless, the change in the number of hydrogen bonds among the water molecules outside the first solvation shell is less than two for all of the solutes studied. The $q=-0.3$ and $+0.5$ solutes are thus not structure breakers in the sense that they reduce the number of bonds among the surrounding water molecules more than the other solutes.

The maxima in the solvation entropy correspond to solutes that ''fit'' into the hydrogen-bond network in the sense that they can replace a water molecule and act either as a double proton donor or as a double proton acceptor; that is, these solutes coordinate tetrahedrally relative to two of the four water molecules in the first hydration shell. Relative to the two remaining water molecules, the solutes coordinate in interstitial (that is nontetrahedral) positions. The fact that these solutes can coordinate in two different ways to each water molecule indicates that they have access to a relatively large set of locations within the hydrogen-bond network. Separation of $S_{\mathrm{sw}}^{(2)}$ into an orientational part and a radial part shows that the orientational part has a single maximum at $q=0$, whereas the radial part has the characteristic bimodal form of the full solvation entropy with maxima at -0.3 and $+0.5$. The water molecules' mass centers are thus less correlated with the $q=-0.3$ and $+0.5$ solutes than with the others, which is consistent with the notion that these solutes have access to a relatively large set of locations within the hydrogen-bond network.

We have characterized the hydration structures surrounding solutes that, in the sense of their solvation entropy, correspond to the extremes of structure making and structure breaking. By comparing these different hydration structures, we have attempted to provide insight into how simple solutes such as noble gas atoms and monovalent atomic ions perturb the spatial and topological structures of water. In particular, since we have compared the extremes, we hope that our results place an upper bound on the size of the perturbations that one can expect.

[1] H. Ohtaki and T. Radnai, Chem. Rev. **93**, 1157 (1993).
[2] G. A. Krestov, *Thermodynamics of solvation* (Horwood, New York, 1991).
[3] F. H. Stillinger, Science **209**, 451 (1980).
[4] R. M. Lynden-Bell and J. C. Rasaiah, J. Chem. Phys. **107**, 1981 (1997).
[5] A. P. Lyubartsev, O. K. Forrisdahl, and A. Laaksonen, J. Chem. Phys. **108**, 227 (1998).
[6] G. Hummer, L. R. Pratt, and A. E. Garcia, J. Phys. Chem. **100**, 1206 (1996).

[7] T. Kowall, F. Foglia, L. Helm, and A. E. Merbach, J. Am. Chem. Soc. **117**, 3790 (1995).
[8] L. X. Dang, J. Chem. Phys. **96**, 6970 (1992).
[9] M. Migliore, G. Corongiu, E. Clementi, and G. C. Lie, J. Chem. Phys. **88**, 7766 (1988).
[10] J. Chandrasekhar, D. C. Spellmeyer, and W. L. Jorgensen, J. Am. Chem. Soc. **106**, 903 (1984).
[11] R. W. Impey, P. A. Madden, and I. R. McDonald, J. Phys. Chem. **87**, 5071 (1983).
[12] W. L. Jorgensen, J. Chem. Phys. **77**, 4156 (1982).
[13] M. Mezei and D. L. Beveridge, J. Chem. Phys. **74**, 622 (1981).
[14] D. L. Beveridge, M. Mezei, P. K. Mehrotra, F. T. Marchese, G. Ravi-Shanker, T. Vasu, and S. Swaminathan, in *Molecular-Based Study of Fluids*, edited by J. M. Haile and G. A. Mansoori (American Chemical Society, Washington, DC, 1983), pp. 304–312.
[15] W. L. Jorgensen, J. Chandrasekhar, J. D. Madura, R. W. Impey, and M. L. Klein, J. Chem. Phys. **79**, 926 (1983).
[16] J. G. Kirkwood and E. M. Boggs, J. Chem. Phys. **10**, 394 (1942).
[17] A. Baranyai and D. J. Evans, Phys. Rev. A **40**, 3817 (1989).
[18] T. Lazaridis and M.E. Paulaitis, J. Phys. Chem. **96**, 3847 (1992).
[19] H. J. C. Berendsen, J. R. Grigera, and T.P. Straatsma, J. Phys. Chem. **91**, 6269 (1987).
[20] S. Nosé, J. Phys.: Condens. Matter **2**, SA115 (1990).
[21] J. P. Ryckaert, G. Ciccotti, and H. J. C. Berendsen, J. Comput. Phys. **23**, 327 (1977).
[22] A. P. Lyubartsev and A. Laaksonen, Lecture Notes Comp. Sci. **1541**, 296 (1998).
[23] S. W. de Leeuw, J. W. Perram, and E. R. Smith, Proc. R. Soc. London, Ser. A **373**, 27 (1980).
[24] L. M. Fraser, W. M. C. Foulkes, G. Rajagopal, R. J. Needs, S. D. Kenny, and A. J. Williamson, Phys. Rev. B **53**, 1814 (1996).
[25] A. P. Lyubartsev, A. A. Martsinovski, S. V. Shevkunov, and P. N. Vorontsov-Velyaminov, J. Chem. Phys. **96**, 1776 (1992).
[26] A. P. Lyubartsev, A. Laaksonen, and P. N. Vorontsov-Velyaminov, Mol. Phys. **82**, 455 (1994).
[27] D. Bergman and A. Laaksonen, Mol. Simul. **20**, 245 (1998).
[28] D. L. Bergman (unpublished).
[29] The program package TOP-PACK [28] was used to analyze the topology of the hydrogen-bond network.
[30] D. L. Bergman and A. Laaksonen, Phys. Rev. E **58**, 4706 (1998).
[31] We have used $g_{OO}(\mathbf{r})$ obtained from the simulation of the pure water system to define the bonds for all solutes.
[32] T. Lazaridis and M. E. Paulaitis, J. Phys. Chem. **98**, 635 (1994).
[33] D. E. Smith, B. B. Laird, and A. D. J. Haymet, J. Phys. Chem. **97**, 5788 (1993).
[34] D. C. Wallace, J. Chem. Phys. **87**, 2282 (1987).